Flow Fields in Electromagnetic Stirring of Rectangular Strands with Linear Inductors: Part II. Computation of Flow Fields in Billets, Blooms, and Slabs of Steel

MATHIAS DUBKE, KARL-HERMANN TACKE,
KARL-HEINZ SPITZER, and KLAUS SCHWERDTFEGER

The model presented in Part I of this series of papers is used to compute flow velocities in the longitudinal stirring of steel blooms and billets, and in the horizontal stirring of steel slabs. In longitudinal stirring of blooms and billets the reverse flow is on the side of the strand opposite to the inductor. The effects of penetration depth of the electromagnetic force, of the force itself, of the length of the stirrer, and of the width of the liquid core were determined. In horizontal stirring of slabs the reverse flow takes place outside of the stirrer region, forming the so-called butterfly stirring pattern. The characteristics of this flow field depend to a considerable extent on the width of the stirrer. The effects of stirrer width, of thickness of the liquid core, of force and of width of the slab were elucidated. The maximum velocities in both types of stirring are represented as simple formulae.

I. INTRODUCTION

In continuous casting of steel electromagnetic stirring is used for improving the solidification structure of the strand. The optimum stirring conditions are usually explored by trial and error. Consequently, it may be helpful to provide fundamentals for the various physical and metallurgical phenomena occurring during stirring. In Part I of this paper[1] a theoretical model has been developed for the computation of flow velocities in rectangular strands stirred by linear inductors. It was tested experimentally using mercury as liquid metal. The agreement between theory and experiments was found to be satisfactory. It was concluded, therefore, that the model is sufficiently reliable to predict flow velocities in steel strands. In this part of the paper the flow fields have been computed for numerous situations of practical interest.

II. LONGITUDINAL STIRRING OF BLOOMS AND BILLETS IN CONTINUOUS CASTING

The flow pattern and the size of the velocity in longitudinal stirring (in or against casting direction) of blooms and billets is influenced by a large number of parameters, *viz.*, geometrical dimensions: length and width of the stirrer, thickness of the solid skin and of the liquid core of the strand, length of sump; electrical quantities: pole pitch, current, voltage, frequency, number of phases; and material properties: electrical conductivity, viscosity, density. More quantities have to be added if another medium (*e.g.*, a copper plate) is located between stirrer and strand. From Part I of the paper it may already be clear that this large number of parameters can be decreased. It was demonstrated[1] that the stirring force of the inductor is completely described, using the theory for an infinitely extended stirrer and a semi-infinite steel medium, by the force existing at the surface of the strand, given by $\sigma\omega B_0^2/(2\lambda)$, and the quantity $Re\gamma$, which depends on λ, σ, and ω according to Eq. [23] of Part I of the paper. (The symbols are explained at the end of the paper.) The number of the remaining parameters, particularly of the geometrical ones, is still so large that it is impossible to present flow patterns for each combination. However, also the variation of single parameters which is carried out in the following, might give useful indications how the stirring process can be optimized.

A. *Optimization of Penetration Depth*

In longitudinal stirring of billets and blooms (Figure 1) the reverse flow takes place at the side opposite to the inductor. This flow is directed against the electromagnetic force. Hence, the force distribution in the liquid core must be so that at the inductor side the force should be high to give stirring action, but at the other side it must be small enough so that the reverse flow is not impeded. (If the force density were constant across the core there would be no stirring at all.) Hence, it is desired to find the force distribution giving an optimum profile of stirring velocity.

The force density decreases exponentially with distance y from the surface of the strand according to[1]

$$F_x = \frac{\sigma\omega}{2\lambda} B_0^2 e^{-2Re\gamma y} \qquad [1]$$

This equation can be written in the form

$$F_x = F_x' e^{-(y-s)/\delta_F} \qquad [2]$$

where F_x' is the time averaged force density at the solidification front $y = s$, and $\delta_F = 1/(2Re\gamma)$.[1] δ_F has the dimension of length and is the distance over which the force decreases (with respect to that at the solidification front) by a factor of $1/e$; it is called "penetration depth".

MATHIAS DUBKE and KARL-HERMANN TACKE, formerly with Institut für Allgemeine Metallurgie, Technische Universität Clausthal, are, respectively, Scientist with Krupp Stahl AG, D-5900, Siegen, Germany, and Scientist with Concast Service Union AG, Toedistr. 7, CH-8027 Zürich, Switzerland. KARL-HEINZ SPITZER, Scientist, and KLAUS SCHWERDTFEGER, Professor, are with Institut für Allgemeine Metallurgie, Technische Universität Clausthal, Robert-Koch-Str. 42, D-3392 Clausthal-Zellerfeld, Germany.

Manuscript submitted July 9, 1986.

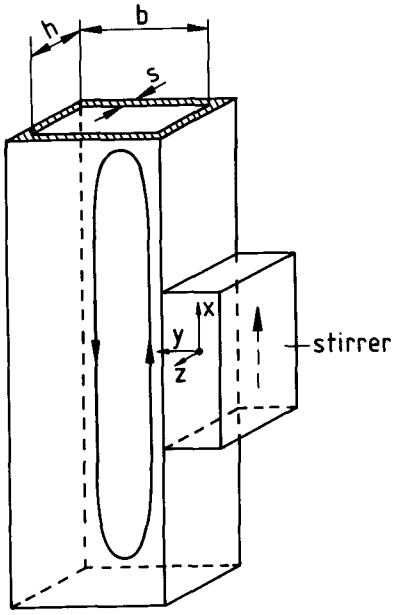

Fig. 1—Longitudinal stirring of billets or blooms (schematical).

$$F_x' = \frac{\sigma\omega}{2\lambda} B_0^2 e^{-s/\delta_F} \qquad [3]$$

$$\delta_F = \frac{1}{2}\left[\frac{\lambda^2}{2} + \frac{1}{2}(\lambda^4 + \sigma^2\mu^2\omega^2)^{1/2}\right]^{-1/2} \qquad [4]$$

Hence, the size of δ_F depends on pole pitch τ of the inductor ($= \pi/\lambda$) and on the angular frequency ω of the electrical current used. Small values of δ_F are obtained at small pole pitch and high frequency, large values at large pole pitch and low frequency.

The computations were carried out with the one-dimensional model (width h of liquid core and length of inductor are infinitely long) for chosen values of force F_x' ($= 1400\ \mathrm{Nm^{-3}}$) and liquid core thickness b ($= 20$ cm). Figure 2 shows examples for the force and velocity profiles at three different values of δ_F. The velocity profile is nonsymmetric, as expected. The location of zero velocity is shifted toward the stirrer side and the difference between the two extrema increases with decreasing δ_F. Figure 3 shows the velocity maximum at the stirrer side as a function of the ratio δ_F/b. The maximum on this curve is located at $\delta_F/b \approx 0.18$, and this position apparently is independent of the stirring force. It is evident that it would be a disadvantage to have a δ_F/b ratio smaller than 0.18 because the velocity decreases steeply at $\delta_F/b < 0.18$. On the other hand, the loss of velocity is not drastic if $\delta_F/b > 0.18$. Hence, to be on the safe side, δ_F/b should be chosen larger than 0.18.

B. *Influence of Length of Stirrer*

The influence of the length L_I of the stirrer is important in two respects. The practical engineer wants to know how far below and above the inductor the stirring reaches. With respect to the theoretical model it is interesting to find out at which L_I the v_x-y profile coincides with that obtained with the one-dimensional computation (setting all derivatives with respect to x and v_y to zero), which can be carried out with less computer time.

Figure 4 shows two-dimensional flow patterns for a billet which is stirred by inductors of two different lengths. Figure 5 gives the x-component of the velocity at a distance of 1.1 cm from the wall (solidification front) as a function of x-coordinate. From both diagrams it is seen that the stirring ends a small distance below the stirrer, but extends a considerable distance in stirring direction. In these computations an apparent problem was encountered because the flow field did not become completely stable at the lower edge of the inductor. A vortex periodically appeared and disappeared there (dashed part of curve). This phenomenon may be numerical. But it may also be real; that is, there may not be a stationary solution to the equations in this region. Also the real turbulent flows can exhibit nonstationary behavior (see Part I, experiments with mercury in shallow bath).

In Figure 6 the values of v_x at $x = 0$ and 1.1 cm from the solidification front are plotted against L_I. The figure also contains a set of data in which L_I was varied to very small values. The very low L_I values are not realistic since in re-

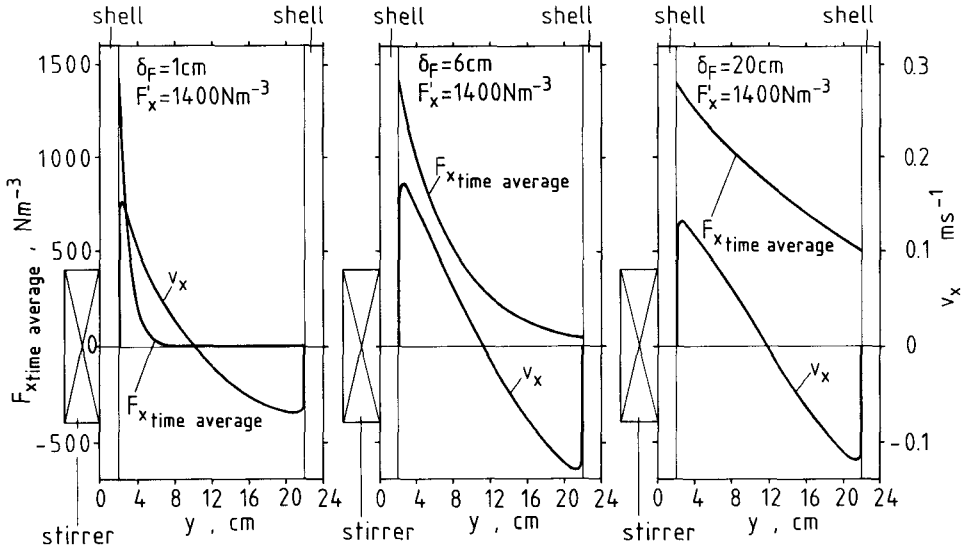

Fig. 2—Profiles of force and velocity at three chosen values of penetration depth in longitudinal stirring of billets and blooms.

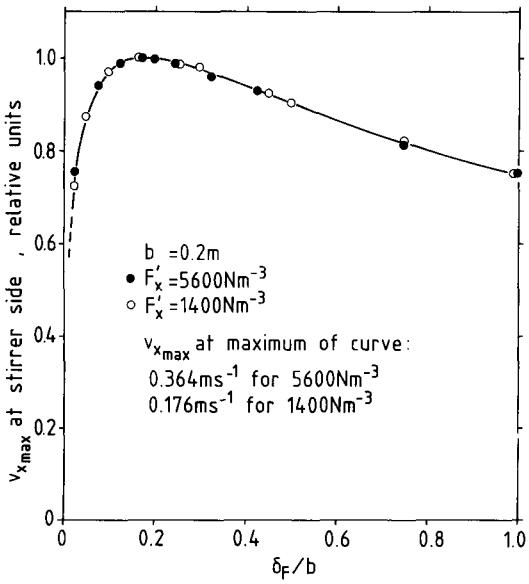

Fig. 3—Maximum velocity at the stirrer side as a function of dimensionless penetration depth in longitudinal stirring of billets and blooms.

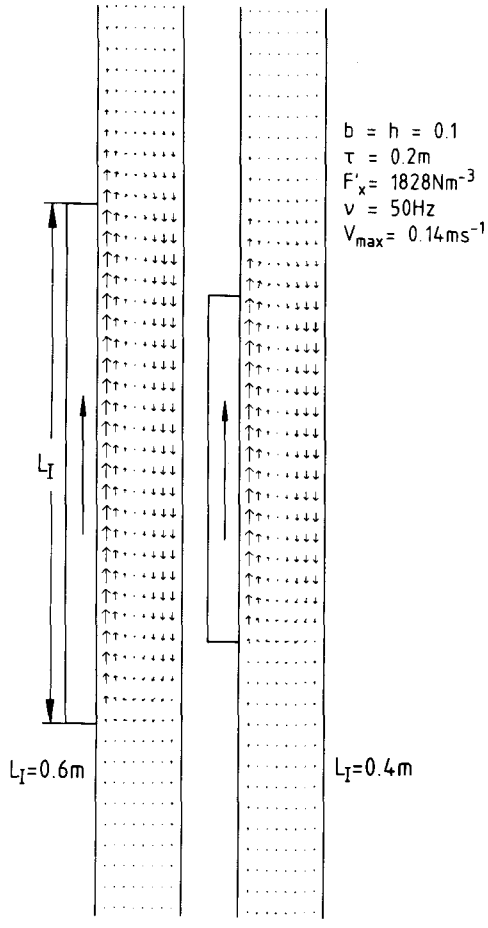

Fig. 4—Flow fields in two billets stirred with inductors of different lengths.

ality the inductor length usually is $\geqq 2\,\tau$; but they could be achieved as effective L_I when a part of the inductor surface is shielded. The velocity decreases, as expected, with decreasing L_I. Included in Figure 6 are the limiting velocity values for the infinitely long stirring system ($L_I \rightarrow \infty$) ob-

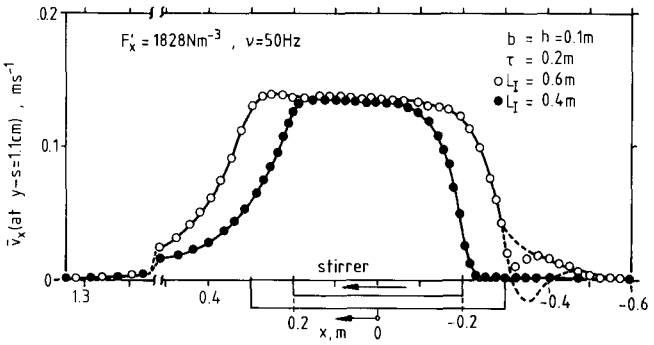

Fig. 5—Longitudinal velocity at 1.1 cm distance from the solidification front in two billets stirred longitudinally with inductors of different lengths.

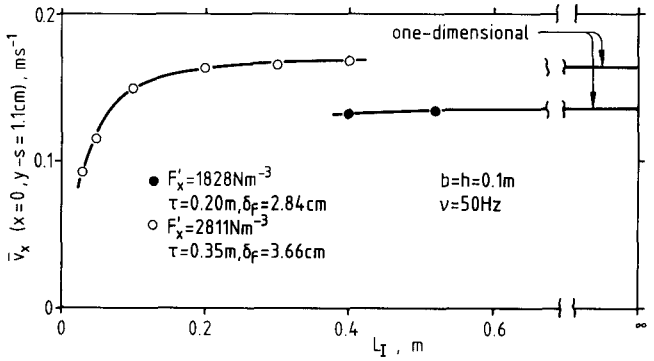

Fig. 6—Longitudinal velocity at $x = 0$ and 1.1 cm distance from the solidification front as a function of stirrer length in longitudinal stirring of billets and blooms.

tained with the one-dimensional model. It is evident that the one-dimensional and two-dimensional results agree for $L_I > 0.2$. Hence, the one-dimensional calculation may predict the maximum velocity value and the v_x-y profile very closely for all the stirrer lengths used in practice.

C. *Influence of Width of Strand (Depth-Averaging)*

The walls at $z_1 = -h/2$ and $z_2 = h/2$ are taken into account by the depth-averaging procedure. It was investigated how small h must become to be of influence. In Figure 7 the maximum velocity value on the $\bar{v}_x$-y profile is plotted *vs* the ratio h/b. It is evident that the influence of the width on the maximum velocity value becomes important when $h/b < 0.4$. Since profiles of $h/b < 0.4$ are not used in steelmaking (billet $h/b = 1$, bloom $h/b > 1$), it may be stated that the effect of strand width on the maximum velocity value is very small in longitudinal stirring of billets and blooms. This is in contrast to the flow-through rectangular ducts,[2] but it can be explained by the fact that the friction controlling the velocity is mainly at the centerplane of the core where forward and reverse flow contact each other, and not at the walls.

Figure 7 contains two curves. One is obtained by applying depth-averaging to all the equations (dashed curve), and the other by applying it only to the equations of motion and of continuity using the equations for k and ε in the non-depth-averaged form (omitting the terms G_K and G_ε in Eqs. [14] and [15] of Part I). In the first case laminarization occurs with decreasing h/b which first leads to an increase

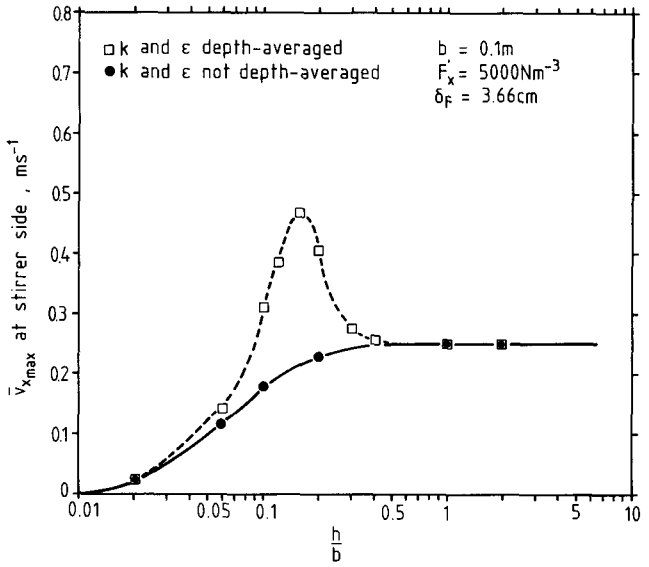

Fig. 7—Maximum value of longitudinal velocity (depth-averaged) as a function of width h in longitudinal stirring of billets and blooms.

of velocity. The model was tested on pipe flow through rectangular pipes in the same h/b range and did not show this effect. An additional two-dimensional model was developed for computing v_x as a function of y and z in an infinitely long strand or pipe. This again yielded the laminarization effect for the MHD problem but not for the pipe flow. So, the present depth-average model is correct for pipe flow, but for the recirculatory MHD flow it appears not to be resolved whether the laminarization is real or an artifact.

D. *Influence of Electromagnetic Force*

Figure 8 shows the effect of the electromagnetic force F'_x on the maximum velocity value existing at the stirrer side. The data are for three different values for the thickness b of the liquid core, but keeping the ratio δ_F/b constant at 0.5. It is evident that the velocity increases approximately linearly with the square root of the force. This is in agreement with the measurements carried out with the mercury model which were described in Part I of the paper, and it is typical for turbulent MHD flow.

E. *Formula for Estimation of Velocity*

It is assumed that the stirrer is sufficiently long and the strand sufficiently wide so that there are no effects of stirrer length and of the side walls. Then, the velocity profile through the strand at the center of the stirrer depends only on F'_x, δ_F, η, ρ, and b, and can be computed with the one-dimensional non-depth averaged program.

It can be shown that the dimensionless force density f (or friction factor) is a sole function of Reynolds number Re and penetration depth ratio δ_F/b. Friction factor and Reynolds number are defined as

$$\mathrm{Re} = \frac{b\rho v_{x\,\max}}{2\eta} \qquad [5]$$

$$f = \frac{F'_x b}{\rho v^2_{x\,\max}} \qquad [6]$$

Figure 9 shows the obtained relationship between f and Re for $\delta_F/b = 0.5$. Two regions can be distinguished. For $\mathrm{Re} < 80$ the flow is laminar and is proportional to $1/\mathrm{Re}$

$$f = \frac{73}{\mathrm{Re}} \qquad \mathrm{Re} < 80 \qquad [7]$$

For $\mathrm{Re} > 250$ the flow is fully turbulent. In between there is a transition range where difficulties existed in the computations due to convergence problems.

In the fully turbulent range f varies approximately linearly with Re in the logarithmic plot up to about $\mathrm{Re} = 10^5$, and can be represented by equation

$$f = 9.04\mathrm{Re}^{-0.175}, \qquad 300 < \mathrm{Re} < 100\,000 \qquad [8]$$

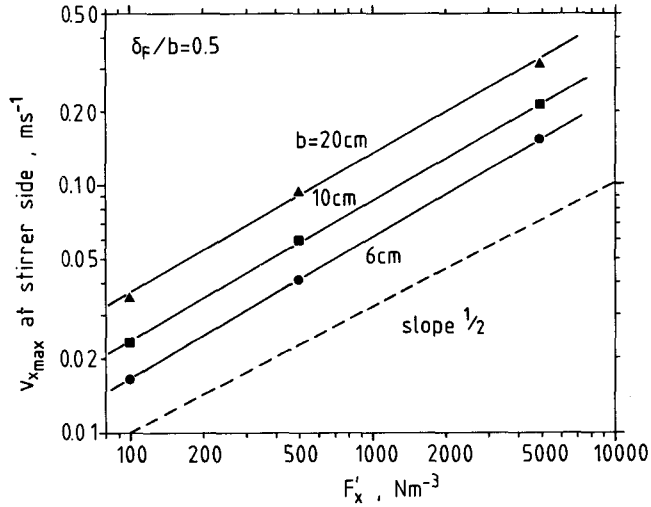

Fig. 8—Maximum value of longitudinal velocity as a function of electromagnetic force density in longitudinal stirring of billets and blooms. Computed without depth-averaging ($h = \infty$).

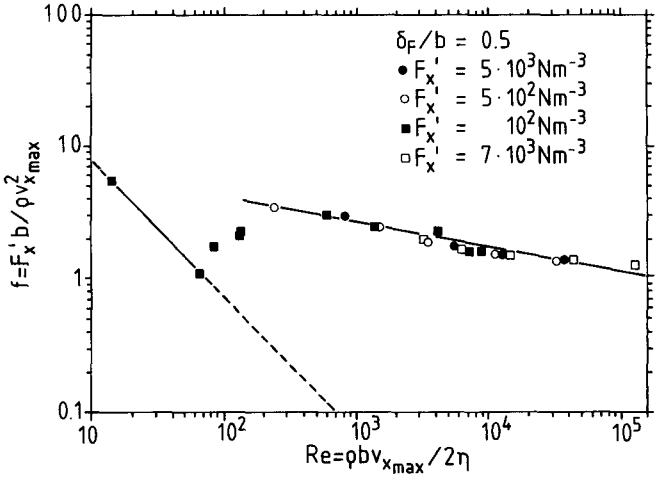

Fig. 9—Dimensionless correlation for stirring velocity in longitudinal stirring of billets and blooms. Velocities were computed without depth-averaging ($h = \infty$).

This expression can be converted to a formula for $v_{x\,max}$

$$v_{x\,max} = 0.280 F_x'^{0.548} b^{0.644} \rho^{-0.452} \eta^{-0.0959} \quad [9]$$

If the numerical values of η and ρ for steel are inserted into Eq. [9], the formula

$$v_{x\,max} = 0.00825 F_x'^{0.548} b^{0.644} \quad [10]$$

is obtained in which $v_{x\,max}$ is in m s^{-1}, F_x' in Nm^{-3}, and b in m.

Equations [9] and [10] are applicable for $\delta_F/b = 0.5$. For other δ_F/b values $v_{x\,max}$ must be multiplied with a correction factor deduced from the curve in Figure 3.

III. HORIZONTAL STIRRING OF SLABS

Slabs are usually stirred horizontally (perpendicularly to casting direction) with one inductor located behind the rolls at the upper side of the strand. The flow pattern is of the butterfly type, as shown schematically in Figure 10. A modification is the system where the inductor coils are placed within rolls. Longitudinal stirring (in casting direction) is not so common with slabs.

In the computation of the stirring force the austenitic rolls must be considered which are located between the strand and the inductor. Presumably, the rolls do not affect the magnetic field in a much different way than an air gap so that Eqs. [26], [27], or [B-25] of Part I can be used. It would be best, of course, to measure the magnetic induction at the surface of the strand and place the origin of the coordinate system there.

In the present work Eq. [27] of Part I was used in the form

$$\overline{F}_x = F_x' \frac{\delta_F}{h}(1 - e^{-h/\delta_F}) \quad [11]$$

where F_x' is again the force density (time average) at the solidification front. Hence, the stirring force is characterized by F_x', by the penetration depth δ_F [$= 1/(2Re\gamma)$], and the thickness h of the liquid sump.

It should be emphasized that in horizontal stirring of slabs the penetration depth must be chosen large so that the decrease of force over the thickness of the liquid core is small. If this is not so, the resulting fluid flow may not be of the desired butterfly type. Instead of this, the reverse flow may be within the region of the stirrer at the other side of the slab (with a z-component of velocity at the narrow sides of the slab), similarly as in longitudinal stirring of blooms and billets. The large penetration depth is obtained by building the inductor with a large pole pitch and by operating it with current frequency lower than 50 Hz (*e.g.*, 2 to 10 Hz).

A. *Influence of Width of Stirrer*

Figure 11 shows the flow pattern for four slabs stirred with inductors of different width from 0.30 to 2.40 m (2.40 m wide inductors are not used in practice). Force density ($\overline{F}_x = 1911$ Nm^{-3}), thickness of liquid region ($h = 0.15$ m), width of liquid region ($= 1$ m), and length of liquid region considered in the calculations ($= 6$ m) are the same. All the flow patterns have the form of a butterfly. But on closer examination there are considerable differences. In Figure 12 the characteristic velocities in the slabs with widest (2.40 m) and with narrowest (0.30 m) inductor are compared. Figure 12(a) shows the horizontal velocity component $\overline{v}_x$ in the longitudinal midplane of the slab ($x = 0$) as a function of longitudinal coordinate y. It is evident that the velocity maximum at the center of the inductor ($y = 0$) is much higher in the slab stirred with the narrow inductor. The reverse flow commences close to the inductor boundaries in the case of the wide inductor, and about one

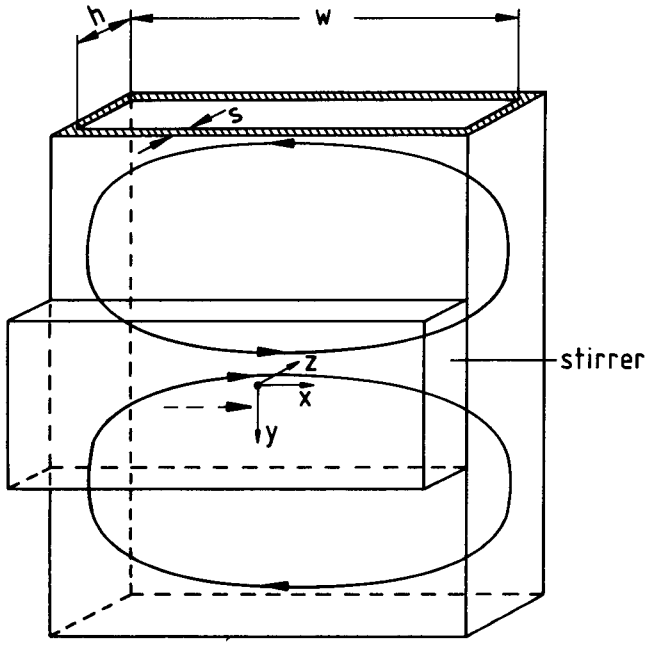

Fig. 10—Horizontal stirring of slabs (schematical).

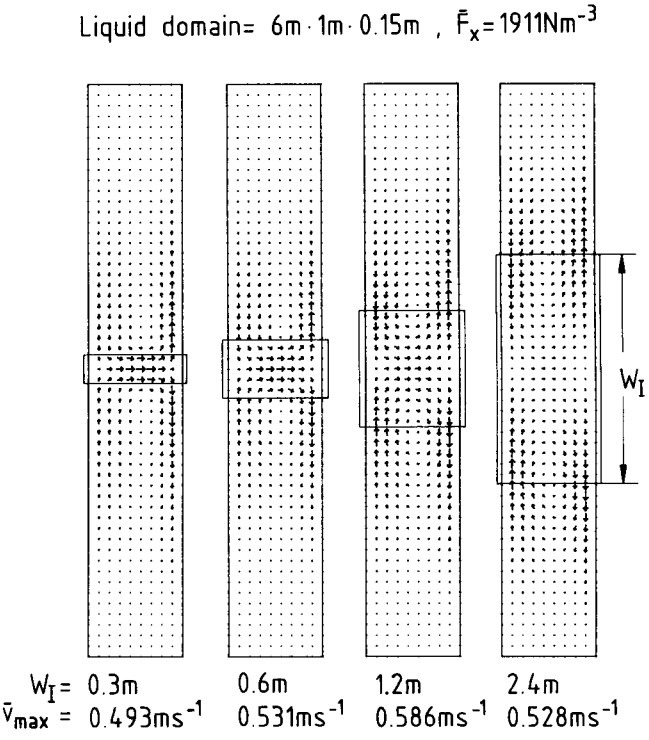

Fig. 11—Flow pattern in slabs stirred horizontally with inductors of different widths.

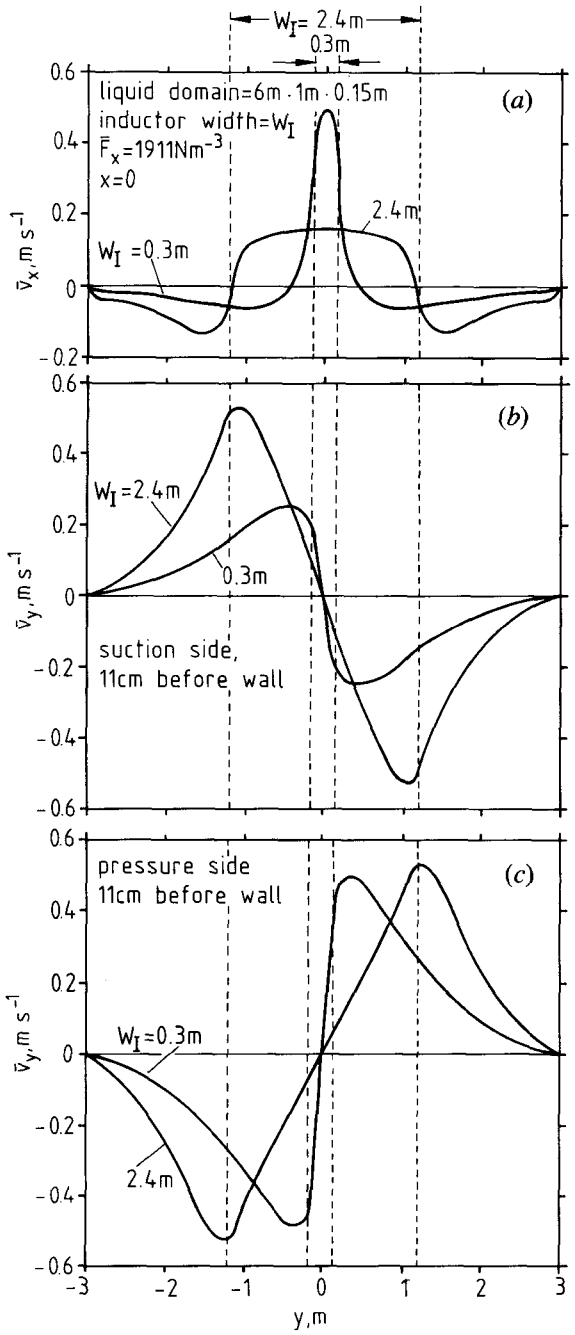

Fig. 12—Characteristic velocity profiles in a slab stirred with a very narrow and with a very wide stirrer.

inductor width away from the inductor in the case of the narrow inductor. The maxima of the reverse flow velocity (minima on curve in Figure 12(a)), however, are larger for the wide inductor than for the narrow inductor. If one assumes that the intensity of the white bands* increases with the flow velocity, it should be expected that one strong and two weak white bands or three weak white bands will develop in the middle of the wide face of the slab, if stirring is with the narrow or wide inductor, respectively.

*White bands are bands of decreased solute content occurring in the solidified strand after electromagnetic stirring.

Figures 12(b) and 12(c) show the longitudinal velocity component $\bar{v}_y$ at 11 cm before the solidification front at the narrow slab faces, both at the suction and at the pressure sides. It is evident that $\bar{v}_y$ is considerably larger at the pressure side than at the suction side, when the inductor is narrow. This agrees with the appearance of the white bands at the narrow sides of the slab which have been reported to be more pronounced at the pressure side.[5] The computations show that this nonsymmetry should decrease when the inductor becomes wider. For the wide inductor the longitudinal velocities $\bar{v}_y$ are much larger than the horizontal velocities $\bar{v}_x$. This may cause the white bands to become stronger at the narrow faces than at the wide faces of the slab.

If the size of stirring velocity is taken to be a measure for the metallurgical effectiveness of the stirrer, the narrow inductors are to be preferred. They make velocity fields with horizontal and longitudinal components of similar magnitude. If the stirring is with a very wide inductor there is a rather still region around the center of the inductor.

The results are summarized in Figure 13 in which the maximum values of both velocity components are plotted against the inductor width W_I.

B. *Influence of Liquid Core Thickness*

Figure 14 shows the influence of thickness h of the liquid region. The width and length of the liquid metal are again 1

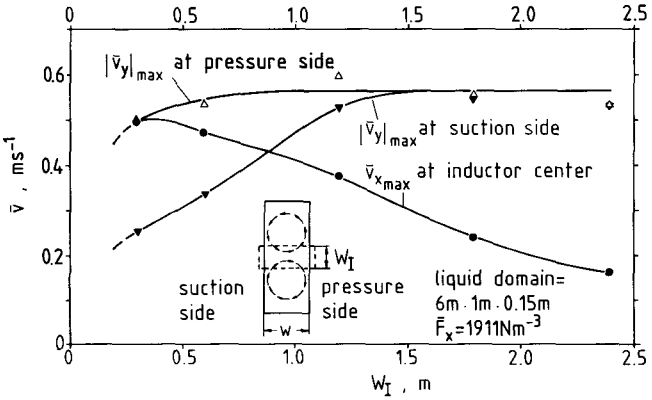

Fig. 13—Maximum value of velocities (absolute value) in the flow field as a function of inductor width for horizontal stirring of slabs.

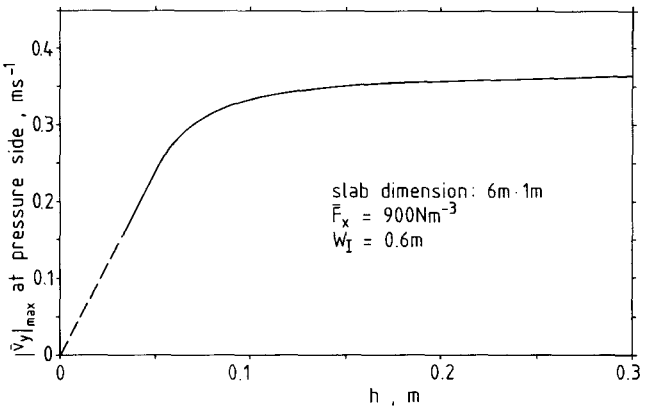

Fig. 14—Influence of liquid core thickness on maximum value of the velocities in the flow field. The maximum velocity value exists, for these geometrical conditions, at the pressure side and is in the y-direction.

and 6 m, respectively, and the width of the stirrer is 0.6 m. It is evident that for $h < 8$ cm the motion is strongly decelerated due to the friction at the side walls, but for $h > 8$ cm a limiting value is soon reached.

C. *Influence of Electromagnetic Force Density*

Figure 15 shows the maximum velocity value as a function of force density $\bar{F}_x$ for three slabs with different sump geometry. The sump thickness h was 0.15 m and the stirrer width $W_I = 0.6$ m. The maximum velocity value exists, for these geometrical conditions, at the pressure side in the y-direction. It is again demonstrated that the velocity increases close to linearly with the square root of force.

D. *Formula for Estimation of Velocity*

It has been shown in the preceding sections that the thickness h of the liquid core (see Figure 14) and the width W_I of the inductor (see Figure 13) have only little influence on the maximum value of stirring velocity ($\bar{v}_y$ at pressure side) when certain values are exceeded, *e.g.*, in the calculated examples $h > 8$ cm, $W_I > 30$ cm. The main factors are then the force $\bar{F}_x$, the width w of the slab, and the material properties ρ and η of the liquid metal. Hence, we can again attempt to represent the maximum velocity value in dimensionless form using the friction factor f and the Reynolds number Re defined as

$$f = \frac{2\bar{F}_x w}{\rho \bar{v}^2_{y\,\max}} \qquad [12]$$

$$\mathrm{Re} = \frac{w\rho|\bar{v}_y|_{\max}}{\eta} \qquad [13]$$

The obtained correlation is shown in Figure 16. The geometrical ratio h/W_I is constant for the data, but the ratio w/W_I is variable. It appears that the influence of w/W_I is not large, as expected, in the range investigated. The line drawn through the points in Figure 16 is represented by

$$f = 5.57\mathrm{Re}^{-0.0731} \qquad [14]$$

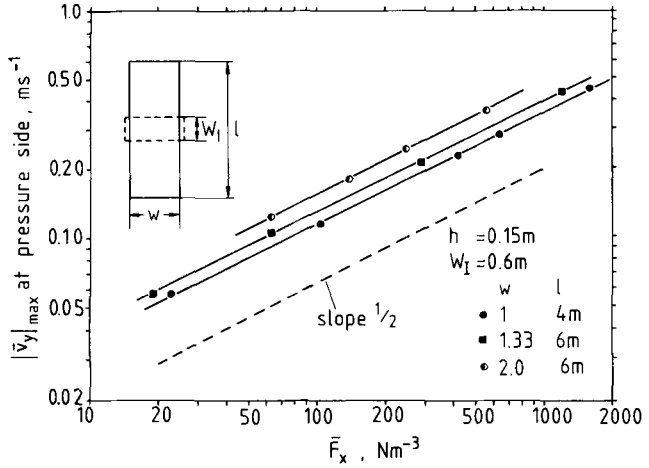

Fig. 15—Maximum value of velocities in the flow field as a function of electromagnetic force. The maximum velocity value exists, for these geometrical conditions, at the pressure side and is in the y-direction.

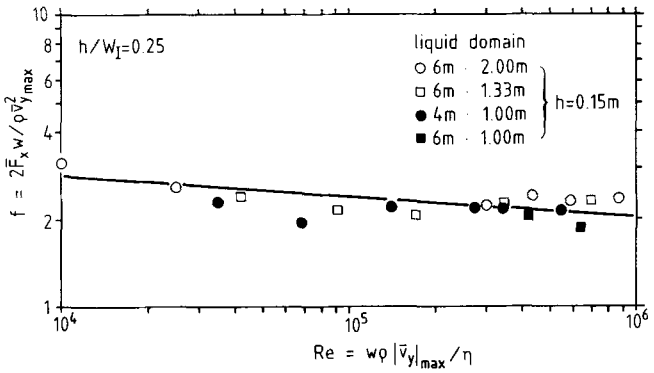

Fig. 16—Dimensionless correlation for stirring velocity in horizontal stirring of slabs.

which is equivalent to

$$|\bar{v}_y|_{\max} = 0.588\bar{F}_x^{\,0.519} w^{0.557} \rho^{-0.481} \eta^{-0.0379} \qquad [15]$$

If the numerical values of η and ρ for steel are inserted in [15], the formula

$$|\bar{v}_y|_{\max} = 0.00995\bar{F}_x^{\,0.519} w^{0.557} \qquad [16]$$

is obtained in which $|\bar{v}_y|_{\max}$ is in m s^{-1}, $\bar{F}_y$ in Nm^{-3}, and w in m. This expression can readily be used to estimate the characteristic velocity value $|\bar{v}_y|_{\max}$.

IV. CONCLUSIONS

In the present work the flow fields in electromagnetic stirring of billets, blooms, and slabs of steel have been computed for numerous situations of practical interest. For the vertical stirring of blooms and billets the influence of penetration depth of the electromagnetic force, of the force itself, of the length of the stirrer and of the width of the strand, and for horizontal stirring of slabs the effect of width of the stirrer, of slab thickness, of slab width, and of the force have been elucidated. The maximum velocity values are given in the form of simple equations. The model used is described in Part I of the paper. It involves the solution of the equations of motion and of continuity. The turbulent viscosity is obtained with the k-ε model. The electromagnetic force is determined from the Maxwell equations. The model is two-dimensional, but the third coordinate can be taken into account by the procedure of depth-averaging. The third coordinate is that over which the velocity component is very small compared to the two other components which is the direction of width in blooms and billets, and of thickness in slabs. The experiments conducted with mercury agree satisfactorily with the theoretical computations. Hence, it is believed that reliable predictions of stirring velocity in steel strands is well possible.

It is known, of course, that the metallurgist is primarily interested in the metallurgical effects of stirring, *e.g.*, in the influence of stirring on the columnar/equiaxed transition during solidification, or in the extent of white band formation. A good model for computing these metallurgical phenomena would be very complex. It would include the solution of the equations for transport of heat and of solute.

The mushy zone would have to be taken into account. There would be a number of assumptions necessary since the processes controlling formation of freely floating crystals and the rheological behavior of two-phase mixtures are not well understood yet. Consequently, it will still take some time till such a complete model will be available. Nevertheless, a model for the flow-field is the prerequisite for making the complete model. So, the present model represents the necessary starting point. It is rather useful already now when different types of stirring are to be compared. For instance, it can easily be determined with the present model how the size of the stirred region would depend on the length or width of the inductor, or how differences in pole pitch could be compensated by other values of magnetic induction, or frequency, and so on.

SYMBOLS USED

b thickness of liquid core in billet or bloom
B magnetic induction
B_0 amplitude of B_y at $y = 0$, or of B_z at $z = 0$
F_x x-component of electromagnetic force density
F'_x x-component of electromagnetic force density at solidification front ($y = s$)
f friction factor
h extension of liquid steel over which depth-averaging is carried out. This is equal to the width of the liquid core in billets and blooms, and to the thickness of the liquid core in slabs.
L_I length of inductor
l length of slab over which computation is carried out
s thickness of solidified shell
Re Reynolds number
$Re\gamma$ real part of γ (see Eq. [23] of Part I)
v_x, v_y velocity components
x, y, z spatial coordinates
w width of liquid core of slab
W_I width of inductor
η dynamic viscosity (0.006 kg m^{-1} s^{-1} for steel)
δ_F penetration depth of electromagnetic force
λ wave vector (π/τ)
ν frequency of current
ω angular velocity of current ($2\pi\nu$)
μ magnetic permeability ($1.2566 \cdot 10^{-6}$ Vs A^{-1} m^{-1})
ρ density (7200 kg m^{-3} for steel)
σ electrical conductivity ($7.14 \cdot 10^5$ AV^{-1} m^{-1} for steel)
τ pole pitch of inductor
- denotes depth-averaged quantity
$| \, |$ absolute value

REFERENCES

1. M. Dubke, K.-H. Tacke, K.-H. Spitzer, and K. Schwerdtfeger: *Metall. Trans. B*, 1988, vol. 19B, pp. 581-93.
2. M. Dubke: Dr. Ing. Thesis, Technische Universität Clausthal, Germany, 1985.
3. C. K. G. Lam and K. Bremhorst: *Trans. ASME*, 1981, vol. 103, pp. 456-60.
4. H. Schlichting: *Boundary Layer Theory*, McGraw-Hill, New York, NY, 1979.
5. T. Shiraiwa, Y. Sugitani, M. Mizutani, S. Kobayashi, I. Susumu, and H. Tomono: *The Sumitomo Research*, Nov. 1979, vol. 22, pp. 97-107.